# Can You See What Others See –A Defect Detection Model for Patterned Backgrounds

*Guo-Feng Wei, M. Ronnier Luo, Peter A. Rhodes, Department of Colour and Imaging Science, University of Leeds, Leeds, UK*

## Abstract

*No one wants defects on their products – neither manufacturers nor consumers. For manufacturers, a series of quality inspection processes is always required to ensure qualities of all their products are under control. For consumers of liquid crystal displays (LCDs), however, they may only concern whether they can see defects on their displays. In this sense, visibility of defects is more important than whether they really exist. Mura is such type of detects on LCDs that most people might have neither heard about it nor been aware of (existence of) them on their panels but some professional users do concern them a lot. This reflects that Mura defects are visually hard to notice and thus tend to be easily overlooked by most users; but in certain circumstances they are really an issue to image quality. In this research, a Mura detection model based on human visual perception was established particularly for visibility prediction of Mura on patterned backgrounds. It is also a model different from current industrial standards which suggest, and therefore are limited to, inspections of Mura defects to be carried out on uniform neutral grey backgrounds. Our analysis showed that colour did not have as much influence on the visibility as previous studies reported when Mura defects are viewed against patterned backgrounds. For a given Mura size and special frequency of a patterned background, there existed a linear relationship between the model outputs (dR, in terms of $\Delta E^*_{ab}$) and the lightness ($L^*$) of the background. An interesting phenomenon was also found that the 1st derivative of the slopes (i.e. slope variation across different experimental conditions) of the linear functions representing the relationships mentioned above can represent the special frequency effect whilst the 2nd derivative of the slopes represents the Mura size effect on the visibility of Mura patterns. Apparently this model provides more reliable predictions of visibility to situations closer to the reality that it is usually complex images, rather than uniform colour patches, are displayed on LCDs. Preliminary analysis also shows that the proposed model can deliver more reliable results for patterned backgrounds than S-CIELAB does.*

## Introduction

For many years, researchers have covered this issue by providing methods to measure Mura defects and proposing visual models to determine whether a Mura pattern is visible under certain conditions. But few of them extended investigations to conditions where Mura defects are viewed against complex images in background. This makes those researches less close to the reality that customers normally watch complex image contents with their LCD's and would barely notice a Mura defect on their displays. From this point of view, it is worth establishing a Mura detection model which involves colour and spatial pattern factors. This work seeks to provide more reliable grading results from experts in agreement with ordinary observers viewing real complex images on LCD's.

An exaggerated image of the Mura defect on a LCD is shown in Figure 1. According to Video Electronics Standards Association (VESA), an industrial standard organization, "Mura defects appear as low contrast, non-uniform brightness regions, typically larger than single pixels." [1]. In fact, Mura defects could be caused by any flaws occurring in any part of the manufacture process as long as they have 'local' influence on, at a later stage when the whole process are finished, the amount of light passing through the LCD panel. These include flaws from light source (backlit lamp) to any components that the light passing through before leaving the panel. All these make Mura defects appear in various shapes and cause slight changes in the transmission property in local areas of the display [2], and it is this subtle nature that results in them being hard to detect by normal optical instruments, although our highly-sensitive visual system can see them with relative ease.

***Figure 1.*** *A typical sample of Mura defect [11]*

For years, researchers have endeavoured to establish a reliable automatic inspection system [3,4] as well as a widely-accepted inspection standard [1,5]. Many studies on Mura detection have also been conducted previously. From those studies, results show that the contrast detection threshold of Mura patterns decreases with display luminance [6,7], which reveals background luminance is one of the dominant factors that affects the visibility of Mura. Compared with the deviation in luminance, however, the spatial gradient of luminance has more influence on the results [8]. Position and size of Mura also play important roles in Mura detection. While there is no surprise that the size of Mura have great influence on its visibility [6,9], it is believed that the influence of position is associated with a masking effect caused by the geographic relationships between Mura and the frames of displays [10]. In the same study, it was also reported that a red background has the greatest visual contrast threshold, followed by green and blue backgrounds. By reviewing the previous studies, it is not difficult to realise that few have extended their investigations into the conditions in which Mura defects are viewed against complex ounds. Research fails to account for the fact that humans, who are capable of processing complex image content, would barely notice a Mura defect on their displays.

## Configuration of the Model

From decades of research, many evidences have shown that our colour vision is pattern-colour separable, indicating that there are three vision pathways in our visual system – one achromatic channel dealing with low spatial frequency signals and two chromatic channels that exhibit band-pass filter characteristics to colour visual signals [12,13]. This is the foundation of our Mura detection model as well as the foundations of S-CIELAB [14] and a model of Ferwada et al. [15] for visual masking in computer graphics applications. Ferwerda et al.'s model also inspired our model in which masking effect is involved.

In order to produce reasonable detection predictions, the Mura detection model comprises four processes that simplify and imitate the procedures occurring in our visual system from the moment an image signal is projected onto the retina to a later stage that masking effect takes place. Here the terms used to describe each process – colour representation, pattern representation, masking and pattern detection were borrowed from Ferwerda et al. [15]. A work flow diagram borrowed from them, representing their model and our model as well is shown in Figure 2.

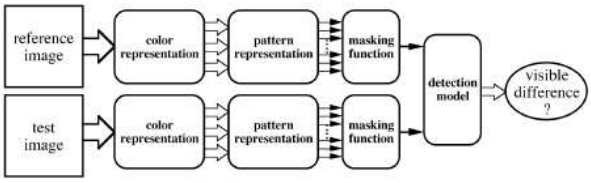


***Figure 2.*** *Components of the masking model proposed by Ferwerda et al. [15]*

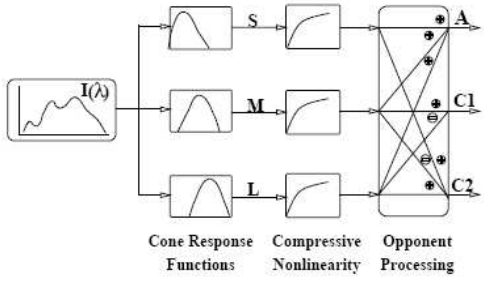


***Figure 3.*** *Illustration of the psychophysical process of colour representation [15].*

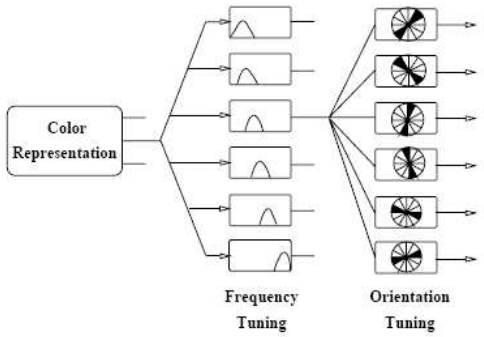


***Figure 4.*** *The pattern presentation where achromatic and chromatic information undergo the same processes for spatial frequency tuning and orientation tuning [15].*

Like s-CIELAB, initially two content-identical images, one with Mura called test image and the other one without Mura on it called reference image, are input into the computational model. The output of this model is the (colour) difference of these two images. In order to provide a more comprehensible prediction result, however, the colour difference is converted into an index with just-noticeable difference (JND) as its unit. Inside the model, four independent computational components are performed step by step to firstly decompose the input image signal into opponent channel information (Fig. 3), and then the result is carried out filtering operations in frequency domain to remove information that is invisible to our visual system (Fig. 4). This filtering operation in Ferwerda et al.'s model [15] comprises two processes dealing with spatial frequency tuning and orientation tuning. Finally the pixel-by-pixel difference of the two input images is summed up in a geometric mean manner to give a quantitative measure of the Mura to our visual system. This value is then converted into JND by applying experimental data as thresholds.

## Experimental Method

An experiment was carried out to collect data for model training. To determine the just notice difference (JND) for different Mura viewed against different types of coloured backgrounds, the method of adjustment [16] was used to accumulate psychophysical visual assessment data acquired in a dark room.

A 22-inch EIZO CG220 LCD was used as the experimental platform in this research. A three-dimensional look-up table (3D-LUT) characterisation model of the display was also established in order to generate desired stimuli for the experiment and to calculate JNDs in terms of colour difference (i.e. $\Delta E^*_{ab}$) for each observer at a later stage. The variables used in this experiment were the type (uniform, isotropic noise), spatial frequency (0, 2, 4 and 10 cpd), orientation (0˚, 45˚ and 90˚), background pattern colour (red, green, blue, yellow, bright grey and dark grey), and size of the simulated Mura (small and large). The patterns of the simulated Mura were defined by the two-dimensional Gaussian function given in Equation (1) [17].

$$\text{Mura}(x,y)=L_0*((1+c)*\exp(-(x^2/\sigma^2))*\exp(-(y^2/2\sigma^2)) \quad (1)$$

where $L_0$ is the local background luminance, c is the contrast and σ is a scaling parameter defining the size of the Mura pattern. In this study, the aspect ratio (height/width) of the Mura patterns was 1.73 whilst the widths (heights) were about 3.3˚ (6˚) and 1.2˚ (2˚), which is equivalent to 0.3 (0.17) cpd and 1 (0.58) cpd, respectively. The noise patterns were luminance-varying and defined in the MacLeod-Boynton domain [18] with contrast of 0.10. Figure 5 illustrates images with different conditions used in this experiment. It also lists the background colours in CIELAB $L^*C^*h$. All the measurements involved in the experiment were carried out using a Minolta CS-1000 tele-spectroradiometer (TSR). There were 14 subjects, 8 males and 6 females, with normal vision (according to the Ishihara test), participating in this experiment. During the experiments, they sat 60 cm away from the display to view a 7.5 $cm^2$ test image surrounded by a neutral background having a brightness of 23.43 $cd/m^2$.

| | BG | DG | R |
|---|---|---|---|
| L*C*h | (68.0,4.0,324.6) | (23.8,0.7,343.1) | (39.6,72.6,43.3) |
| | G | B | Y |
| L*C*h | (48.6,78.1,144.4) | (21.6,52.7,300.5) | (89.0,94.1,98.7) |

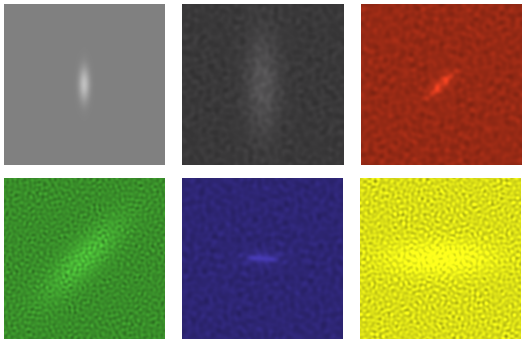

***Figure 5.*** *Illustration of Mura on noisy backgrounds with various spatial frequencies. The CIELAB L*C*h values of these coloured backgrounds are provided above.*

## Results

Figure 6 shows the JNDs in terms of $\Delta E^*_{ab}$ for all experimental conditions and includes one standard deviation error bars. There are three things/points worth noting. First, there is a consistent trend that the JNDs of all colours follow this order: yellow ≈ green ≈ red > blue ≈ bright grey > dark grey. It seems that colour had influence on the results. But further analysis showed that it was the achromatic component of the stimuli, not the chromatic ones, which dominated the trend. More details about this will be provided and explained later in the model training section. Second, masking effect is significant as shown in Figure 7. In this figure, colour influence is removed by applying an average operation over the results out of all colours, i.e. the JNDs for different colour conditions were combined. The reason this can be done is because of the consistent trend mentioned above. This provides a clearer view of the size and masking effect. As can be seen, the masking effect for spatial frequency tunings is significant while the spatial frequencies of Mura are close to that of the backgrounds, i.e. 0.3 cpd for the large Mura and 1 cpd for the small Mura. Mura size has a mild influence on detection against different backgrounds; the difference is about 0.2-0.5 $\Delta E^*_{ab}$ greater for large Mura. Last, orientation effect can be ignored as shown in Figure 7. In summary, JND values obtained here range from 0.3-3.5 $\Delta E^*_{ab}$.

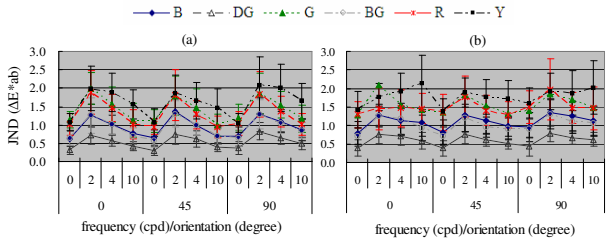


***Figure 6.*** *JNDs of (a) small and (b) large Mura on noisy background.*

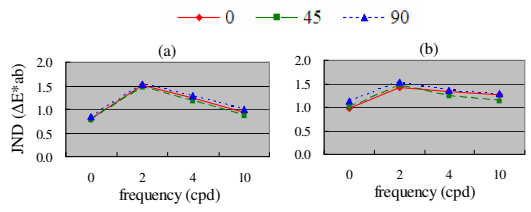


***Figure 7.*** *Mean JNDs of (a) small and (b) large Mura on noisy background.*

## Parameters for Model Training

To make the model work, there are three things need to be included in the training task: colour effect, masking effect on spatial frequency tuning and masking effect on orientation tuning – the results shown previously have revealed these requirements. Figure 8 shows the outputs obtained by the original model for all the experimental conditions with noisy backgrounds. Apparently there is a linear relationship between the colour type and the computational results. Since colour itself can be further decomposed into one achromatic and two chromatic channels, a reasonable assumption was made that it was the achromatic component, i.e. the lightness, of the colour information which gave the trend in Figure 8(a), and this assumption was proved valid in Figure 8(b) when the outputs were plotted against lightness of each colour type. In Figure 9 there are new plots which show the relationship between the model outputs and lightness of the backgrounds. As can be seen in these plots, the linear functions show good agreements with the data with high correlation coefficients. The only difference between different spatial frequency conditions is their slopes. This can be used as a starting point for the model training work.

As mentioned earlier, a process called pattern representation in our detection model manages to decompose colour representation into several individual parts. The knowledge behind this is that our visual system processes spatial patterns with mechanisms tuning to various ranges of frequencies and orientations [19,20]. At this stage, achromatic and chromatic information undergoes the same processes for spatial frequency tuning and orientation tuning as shown in Figure 4. From a modern signal processing point of view, these visual mechanisms serve as filters that filter spatial patterns. Through this process, a spatial pattern can theoretically be discomposed into several individual parts (not necessarily independent with each other); those containing Mura pattern information are extracted and used for Mura discrimination.

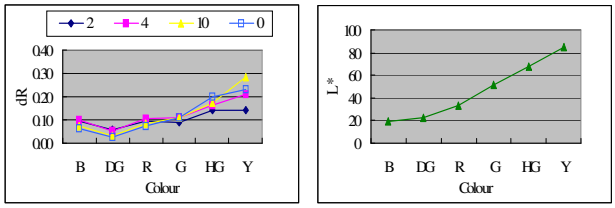


***Figure 8.*** *(a) Model responses vs. background colour for small Mura and (b) the relationship between lightness and the colours used in the experiment.*

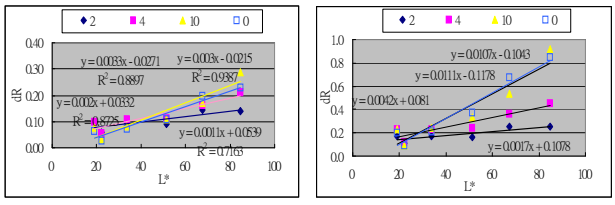


***Figure 9.*** *Model responses for (a) the small Mura (b) the large Mura.*

Wilson and Gelb [20] proposed a line-element theory to model the six mechanisms in the visual system (Fig. 10). In their model, the spatial-sensitivity profile was designated LSF(x) and its Fourier transform was denoted as T{LSF}. They are shown in Equation (2) and Equation (3) as follows. Values of constants, except constant A, for these two equations are provided in Table 1. As suggested by Wilson and Gelb [20],

"*values for the parameter A, which determines the absolute sensitivity of each mechanism,..... were chosen to fit threshold-sensitivity data for each of the different types of patterns and temporal conditions used in various discrimination studies.*"

$$LSF(x) = A \cdot [e^{-(x^2/\sigma_1^2)} - B \cdot e^{-(x^2/\sigma_2^2)} + C \cdot e^{-(x^2/\sigma_3^2)}] \quad (2)$$

$$T\{LSF\} = A \cdot \pi^{0.5} [\sigma_1 e^{-(\pi\sigma_1\omega)^2} - B \cdot \sigma_2 e^{-(\pi\sigma_2\omega)^2} + C \cdot \sigma_3 e^{-(\pi\sigma_3\omega)^2}] \quad (3)$$

Since the six mechanisms all together form the envelope of the human visual contrast sensitivity function, the equations (Eq.4 and Eq.5) and their corresponding parameters (shown in Table 2) suggested by Johnson and Fairchild [21] can be used in conjunction with the peak frequencies listed in Table 1 to determine the parameter A in Equation 3.

$$csf_{lum}(f) = a_1 \cdot f^{c_1} \cdot e^{-b_1 \cdot f} \quad (4)$$

$$csf_{chrom}(f) = a_1 \cdot e^{-b_1 \cdot f^{c1}} + a_2 \cdot e^{-b_2 \cdot f^{c2}} \quad (5)$$

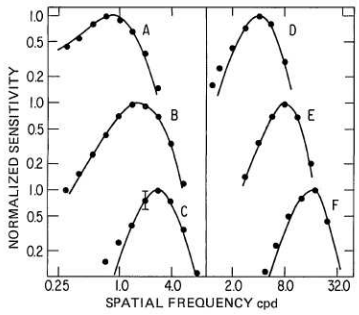


***Figure 10.*** *Spatial frequency sensitivities of the six mechanisms fit to the oblique masking data by Wilson and Gelb [20].*

**Table 1. Values of constants defined by Wilson et al. for the spatial and spatial-frequency sensitivity for each mechanism [19].**

| Mechanism | Peak Frequency (cpd) | B | C | $\sigma_1$ (deg) | $\sigma_2$ (deg) | $\sigma_3$ (deg) |
|---|---|---|---|---|---|---|
| $M_A$ | 0.8 | 0.267 | - | 0.198 | 0.539 | - |
| $M_B$ | 1.7 | 0.333 | - | 0.098 | 0.294 | - |
| $M_C$ | 2.8 | 0.894 | 0.333 | 0.084 | 0.189 | 0.253 |
| $M_D$ | 4.0 | 0.894 | 0.333 | 0.059 | 0.132 | 0.177 |
| $M_E$ | 8.0 | 1.266 | 0.500 | 0.038 | 0.060 | 0.076 |
| $M_F$ | 16.0 | 1.266 | 0.500 | 0.019 | 0.030 | 0.038 |

**Table 2. Parameters for achromatic and chromatic CSFs by Johnson and Fairchild [21].**

| Parameter | achromatic | Red-Green | Blue-yellow |
|---|---|---|---|
| a1 | 75 | 109.1413 | 7.0328 |
| b1 | 0.2 | 0.0004 | 0.0000 |
| c1 | 0.8 | 3.4244 | 4.2582 |
| a2 | - | 93.5971 | 40.6910 |
| b2 | - | 0.0037 | 0.1039 |
| c2 | - | 2.1677 | 1.6487 |

The results in Figure 8 were obtained from the concept mentioned above. In order to give the model some degree of freedoms to meet/reflect the visual responses in our experiment, a set of weighting factors for the visual mechanisms were added in Equation 3 to adjust the absolute sensitivity of each mechanism. Therefore the achromatic CSF is rewritten as follows.

$$CSF = WF_1 * M_A + WF_2 * M_B + WF_3 * M_C + WF_4 * M_D + WF_5 * M_E + WF_6 * M_F \quad (6)$$

where $M_A$ to $M_F$ denote the six mechanisms while $WF_1$ to $WF_6$ are weighting factors for each mechanism. By applying different weighting factors, the influence as well as output of the model can be investigated. In Figure 11 two sets of data labeled "[0.5 0.5]" and "[0.5 1.0]" represent the results for spatial frequency of 2.0 cpd using WF= [0.5 0.5 0.5 0.5 0.5 0.5] and WF= [0.5 1.0 0.5 1.0 0.5 1.0] respectively. As can be seen, changing values of the weighting factors had no influence on the slopes of the data trends but shifted the absolute values of the whole data sets. This implies two things. First, value of 1.0 can be used for all weighting factors, which implies that the CSFs given by previous researchers have shown their suitability in our model. Second, the purposely chosen values of [0.5 1.0 0.5 1.0 0.5 1.0] for WF show that the model is insensitive to variation of individual visual mechanism. Thus a new approach to adjusting/training the model might be necessary.

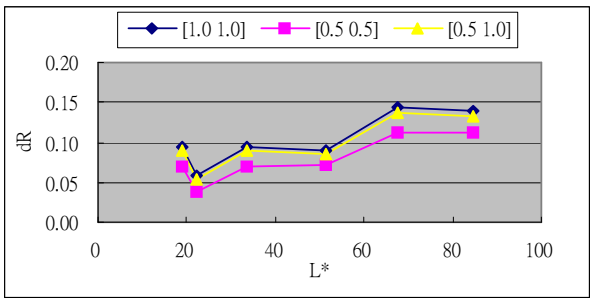


***Figure 11.*** *Model responses with different values of weighting factors.*

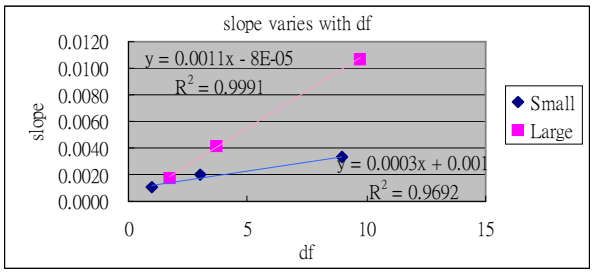


***Figure 12.*** *Slope variations for the small and large Mura.*

Figure 8 shows the initial outputs obtained without any parameters added in the model, and they are named the raw responses of the model. Apparently there are linear relationships between dR and $L^*$ and only the slope changes with the eccentricity of masking frequency, i.e. the difference of spatial frequency between the targets and the backgrounds. This implies that a simple linear function can be used to yield the output if the input is provided. Furthermore the changing rates represented by the slopes of each linear function (except the slope for 0 cpd condition) are shown in Figure 12. Very high correlation coefficients ($R^2$= 0.97 and $R^2$= 0.99) for the small and the large Mura again indicate that the slopes in Figure 9 changes linearly with the eccentricity of masking frequency. At the moment these two phenomena suffice to establish criteria of JND values for inputs with different lightness. With theses

values as a baseline, responses for 2 JND and 3 JND are then used to generate a scale for different eccentricities of masking frequency. This reveals a simple fact which was observed from our experimental data that the human visual system responses differently when the eccentricity of masking frequency or Mura intensity varies under fixed lightness and Mura size condition. A summary is given as below to show how spatial-frequency eccentricity and Mura size affect the output:

*The 1st derivative of the slopes represents the frequency effect whilst the 2nd derivative of the slopes represents the Mura size effect.*

Following this idea, the responses (dR) representing different JND values are plotted against lightness ($L^*$) in Figure 13 and Figure 14. In addition to the good agreement between the linear functions and the data from all inputs, all three trend lines in one plot intersect closely at one point under all spatial frequency conditions. These intersections can be described by a pair of equations and can be calculated for a given eccentricity of the masking frequency. The equations are shown as follows and their curves are plotted in Figure 15 and Figure 16. In these equations ε denotes eccentricity of masking frequency.

$$dR\_small = 0.0018*\varepsilon^2 - 0.0275*\varepsilon + 0.0118 \quad (7)$$

$$L^*\_small = -0.2648*\varepsilon^2 + 6.3991*\varepsilon - 42.37 \quad (8)$$

$$dR\_large = 0.0002*\varepsilon^2 - 0.0242*\varepsilon + 0.0393 \quad (9)$$

$$L^*\_large = -0.8586*\varepsilon^2 + 12.719*\varepsilon - 39.996 \quad (10)$$

The logic behind the model is that: when the spatial frequency of the background is given, it basically determines how responses change with background lightness – as one of the straight lines shown in Figure 9. This can be treated as a viewing condition factor for our visual system which causes a bias or shifts our visual response to a certain level. Then the intensity of Mura, a target as well as a stimulus, determines the final state of our visual response. The influence of the Mura intensity in the model can be observed in Figure 17. For a given masking frequency, the slope of a linear function which describes the responses under different lightness conditions increases linearly with JND values. Note that the linear behaviour stemming from an assumption made for the model is based on the Weber's law. Once the slope of the linear function under a certain viewing condition is known, the linear function can be determined. Here, the visual response (dR) can be calculated according to the input lightness of a background image. Therefore when eccentricity of masking frequency, lightness of background image and Mura intensity are provided, the visual response can be predicted by the model.

In order to make the output values more comprehensible, however, outputs of the model need to be presented in JND values. This requires a new scale built in terms of JND. The whole concept for training the model can be treated this way: to establish 1 JND thresholds as references and then to establish equations that can truthfully represent the behaviour how our visual system reacts when the intensity of Mura increases. And this was achieved by assuming that the response increases linearly with the input intensity. The final modified results in terms of JND values for the small Mura are shown in Figure 17. The target is to have JND values as close as 1.0. As can be seen in this figure, this model has a more stable prediction for stimuli with averaged lightness above 30cd/m$^2$.

## Performance of the Model

S-CIELAB [14] is known as a useful tool in measuring colour reproduction errors of digital images. The advantage of S-CIELAB over CIELAB is that it takes into account characteristics of the spatial vision of our visual system by applying a spatial filtering pre-processing step in an opponent color space. Therefore outputs of S-CIELAB are believed to have a more accurate prediction in image errors. To benchmark the performance of our model, a comparison between S-CIELAB and our model was made. Figure 19 shows the result of the comparison on the small Mura. The results of 0 cpd is removed in order to make the figure clear to read. Results of 2, 4 cpd (small eccentricity of masking frequency) and 10 cpd (large eccentricity of masking frequency) are shown to provide an observation on how these two models perform when masking effect takes place. Apparently our model tends to produce larger values than S-CIELAB, which reflects the fact that observers usually need higher intensity of stimulus to perceive Mura defects when visual masking effect occurs.

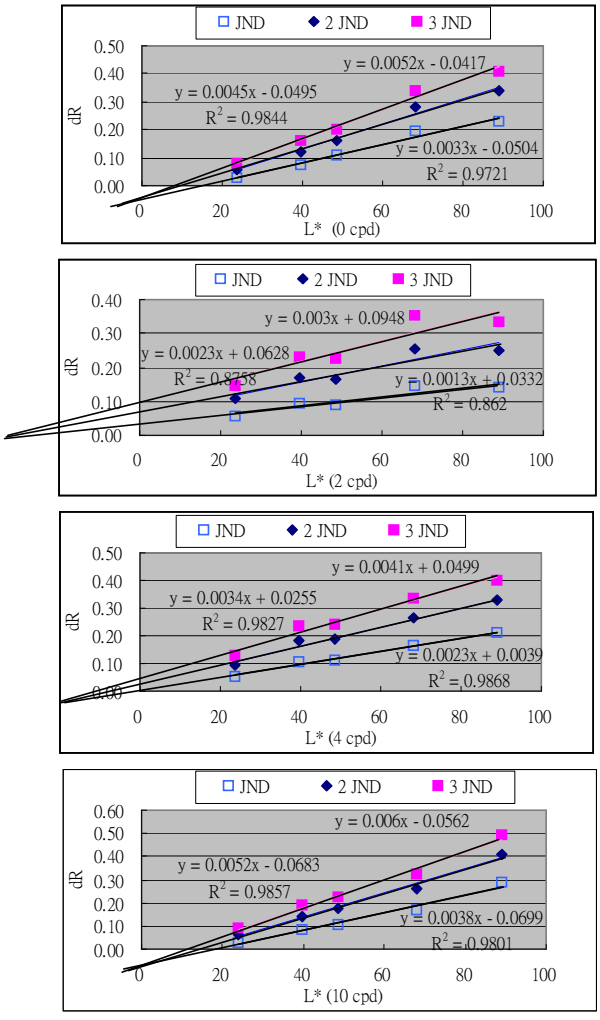


***Figure 13.*** *Variations of model responses for small Mura as its intensity increases in terms of JND. Each plot represents results of a specific background spatial frequency.*

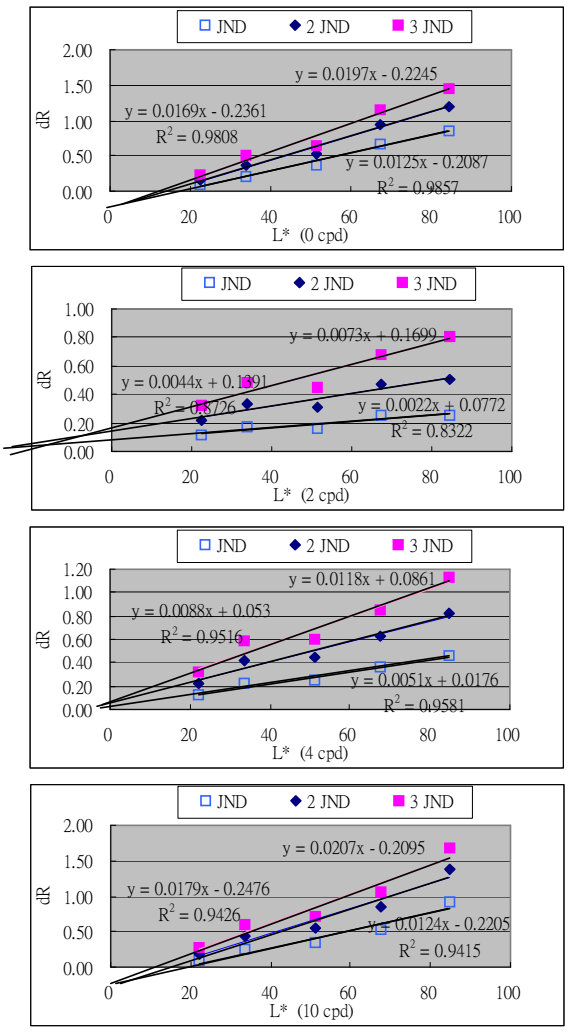


***Figure 14.*** *Variations of model responses for large Mura as its intensity increases in terms of JND. Each plot represents results of a specific background spatial frequency.*

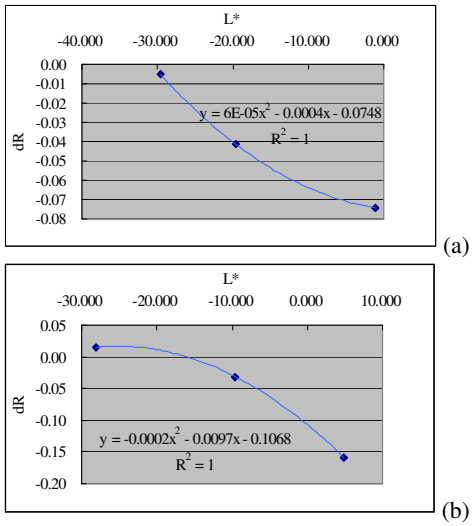


***Figure 15.*** *Intersections of different JND trend-lines for (a) the small Mura and (b) the large Mura.*

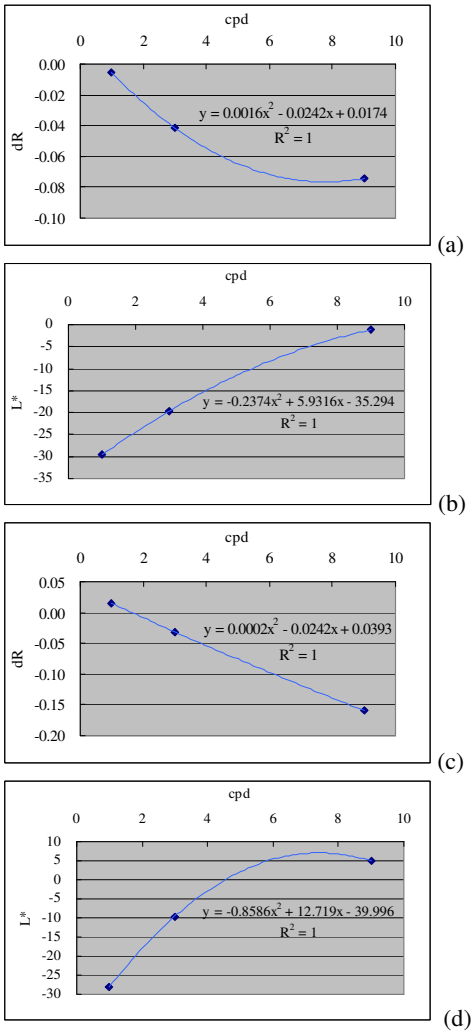


***Figure 16.*** *Intersections of JND trend-lines for (a) dR vs. frequency (small Mura) (b) L* vs. frequency (small Mura) (c) dR vs. frequency (large Mura) (d) L* vs. frequency (large Mura)*

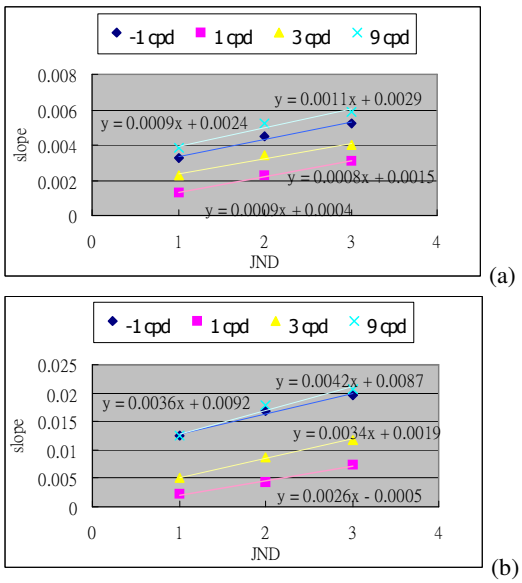


***Figure 17.*** *The influence of the Mura intensity in the model for (a) the small Mura and (b) the large Mura. For a given masking frequency, the slope of a linear function which can represent the model responses under different lightness conditions increases linearly with JND values.*

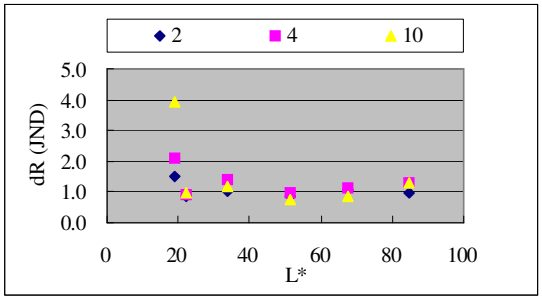


***Figure 18.*** *Modified results in terms of JND values for the small Mura.*

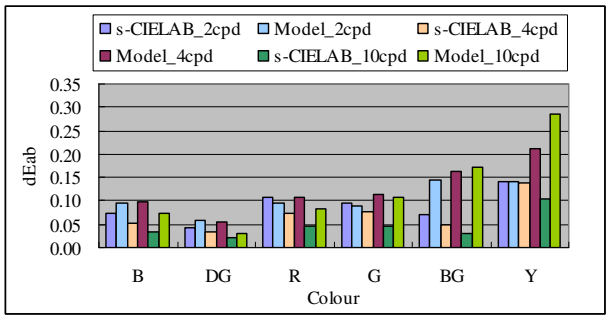


***Figure 19.*** *Comparison of the performance between S-CIELAB and our model.*

## Conclusions

Colour does not have as much influence on the visibility as previous studies reported when Mura defects are viewed against patterned backgrounds. Evidence also showed that the proposed Mura detection model can provide more reliable predictions for Mura visibility on patterned backgrounds than S-CIELAB. The main reason which causes this difference is that S-CIELAB does not take masking effect into consideration. Therefore S-CIELAB tends to underestimate the image difference required to make Mura defects visible.

## References

[1] VESA, Flat Panel Display Measurements Standard Ver. 2.0, (2001).

[2] S.S. Sawkar, J. Hawthorne, C. H. Teh, B. Dutton, R. Mckuhen, G. Alonzo, M. Yamada, M. Nouda, J. Monkowski, and G. Addiego, “Automated Inspection and Classification of Mura Defects in Liquid-Crystal Flat-Panel Displays” SID 94 Digest, 759-763 (1994).

[3] V. Gibour, and T. Leroux. 2003. Automated, Eye-like Analysis of MURA Defects. In *SID 03 Digest*, Campbell, U.S.A. IS&T. 1440-1443.

[4] Y. Mori, K. Tanahashi, R. Yoshitake, T. Tamura, K. Moriguchi, T. Yoshizawa and S. Tsuji. Measurement System and Detection Method of “mura” in TFT-LCD. In *Proceedings of IDMC 2003*, Taipei, Taiwan. IS&T. 295-298. (2003).

[5] SEMI. Definition of Measurement Index (SEMU) for Luminance Mura in FPD Image Quality Inspection, SEMI D31-1102. (2002).

[6] D. G. Lee, I. H. Kim, M. C. Jeong, B. K. Oh, and W. Y. Kim, Mura Analysis Method by Using JND Luminance And the SEMU Definition, Proceedings of SID, pg. 1467-1470. (2003).

[7] T. Tamura, T. Satoh, T. Uchida and T. Furuhata, “Quantitative Evaluation of Luminance Nonuniformity Mura in LCDs Based on Just Noticeable Difference (JND) Contrast at Various Background Luminances” IEICE Trans. Electron, Vol. E89-C, pg. 1435-1440. (2006).

[8] J. H. Kim, “Human Vision-based Detection of Nonuniform Brightness on Liquid Crystal Display Panels” Journal of Electron. Imaging, Vol. 17(3), 1-7. (2008).

[9] C. C. Chen, S.L. Hwang and C.H. Wen, “Measurement of human visual perception for mura with some features,” Journal of the SID 16/9, 969–976. (2008).

[10] P. C. Wang, S. L. Hwang and C. H. Wen. “A Study of Human Vision Inspection for Mura” Human-Computer Interaction. HCII 2007, Volume 4552/2007, 747-754. (2007)

[11] Photon Dynamics, Inc. (PDI), TechNote: Mura Tool, (2000).

[12] Hering E. Outlines of a Theory of the Light Sense. Cambridge, MA: Harvard University Press; 1878/1964.

[13] AB Poirson, BA Wandell. The appearance of colored patterns: pattern-color separability. J Opt Soc A; 10: 2458–2470. (1993).

[14] XM. Zhang, BA Wandell. A spatial extension to CIELAB for digital color image reproduction. Soc for Info Disp Symp Tech Digest 1996; 27:731–734.

[15] J. A. Ferwerda, P. Shirley, S. N. Pattanaik, D. P. Greenberg “A Model of Visual Masking for Computer Graphics” Proceedings of the 24th annual conference on Computer graphics and interactive techniques, pp. 143-152. (1997).

[16] Engeldrum, P. G., Psychometric Scaling: a Toolkit for Imaging Systems Development. Winchester, MA.:Imcotek Press. (2000).

[17] C. C. Chen, S.Y. Lin, H. Y. Han, S. T. Kuo and K. C. Huang. Local luminance effect on spatial summation in the foveal vision and its implication on image artifact classification. In *Proceedings of SPIE,* ed. by B. E. Rogowitz, T. N. Pappas, S. J. Daly. Bellingham, U.S.A. Vol. 6057, 13-21. (2006).

[18] D. I. A. MacLeod, and R. M. Boynton, Chromaticity diagram showing cone excitation by stimuli of equal luminance. *Journal of the Optical Society of America* 69: 1183-1186. (1979).

[19] H. R. Wilson, D. K. McFarlane and G. C. Phillips “Spatial tuning of orientation selective units estimated by oblique masking” Vision Res. 23, 873-882. (1983).

[20] H.R. Wilson, and D.J. Gelb “Modified line-element theory for spatial-frequency and width discrimination” Journal of Optician (Society of America), A (1): 124-131. (1984).

[21] G.M. Johnson and M.D. Fairchild, "A top down description of S-CIELAB and CIEDE2000," Color Research and Application, 28 425-435 (2003).

## Author Biography

*Guo-Feng Wei received his B.S. and M.S. from Department of Power Mechanical Engineering, National Tsing Hua University, Hsinchu, Taiwan in 1997 and 1999, respectively. He is currently a doctoral student at University of Leeds, UK. His research interests include high-dynamic range photography and color management for LCDs.*

.